Received July 15, 2019, accepted July 24, 2019, date of publication July 29, 2019, date of current version August 13, 2019.

Digital Object Identifier 10.1109/ACCESS.2019.2931581

An Enhanced High-Order Variational Model Based on Speckle Noise Removal With G^0 Distribution

YUNPING MU[1], BAOXIANG HUANG[1], (Member, IEEE), ZHENKUAN PAN[1], HUAN YANG[1], (Member, IEEE), GUOJIA HOU[1], AND JINMING DUAN[2]

[1]College of Computer Science and Technology, Qingdao University, Qingdao 266071, China
[2]School of Computer Science, University of Birmingham, Birmingham B15 2TT, U.K.

Corresponding author: Baoxiang Huang (hbx3726@163.com)

This work was supported in part by the National Natural Science Foundation of China under Grant 61602269, in part by the Natural Science Foundation of Shandong Province, China, under Grant ZR2017MD004, in part by the China Postdoctoral Science Foundation under Grant 2015M571993, and in part by the Young Teachers' Growth Plan of Shandong Province.

ABSTRACT Speckle noise removal problem has been researched under the framework of regularization-based approaches. The regularizer is normally defined as total variation (TV) that induces staircase effect. Although higher-order regularizer can conquer the staircase effect to some extent, it often leads to blurred. Considering the upper questions, the combination of first and second-order regularizer will be an effective and prior method to tackle speckle noise removal. So a variational model with hybrid TV and higher-order total curvature (TC) term is proposed in this paper, the data fidelity term is derived based on G^0 distribution. In order to preserve the edge detail better, the boundary detection function is combined with the regularizer. Furthermore, the Mellin transform is used to estimate the parameters of the model. To address the speckle noise removal optimization problem, alternating direction method of multipliers (ADMM) framework is employed to design a convex numerical method for the proposed model. The numerical method can be used to update the variables flexibly as required by the hybrid regularizer. The numerous experiments were performed on both synthetic and real SAR images. Compared with some classical and state-of-the-art SAR despeckling methods, experiment results demonstrate the improved performance of the proposed method, including that speckle noise can be removed effectively, and staircase effect can be prevented while preserving image feature.

INDEX TERMS Speckle noise, synthetic aperture radar (SAR), G^0 distribution, total variation(TV), total curvature(TC), boundary detection function, alternating direction method of multipliers (ADMM), Mellin transform.

I. INTRODUCTION

Synthetic Aperture Radar(SAR) [1] is a high resolution microwave imaging using synthetic aperture principle. Because of the advantages of all-day time, all-weather and high resolution, SAR is widely used in military and civilian fields [2]. SAR imaging system is based on coherence principle which leads to the speckle noise [3]–[5]. In other words, speckle noise is caused by the fading of radar target echo signal. The existence of speckle noise reduces the image quality and seriously affects the automatic image segmentation, classification, target detection and other quantitative thematic information extraction. Consequently, the reduction of speckle noise is a fundamental step in SAR image processing [6].

Speckle noise is non-Gaussian, signal and spatially independent [7], [8], comparing with the additive noise removal [9], [10], the removal of speckle noise is a very challenging task. A variety of approaches have been proposed to despeckle SAR images in the past three decades, such as traditional filtering [11], wavelet-based approaches [12], nonlocal mean (NLM) filtering [13] and variational methods [6]. Among them, traditional filters such as Lee [14] and Kuan [15] filter can perform well in speckle suppression but their effects usually depend on the size and direction of the mask. Besides, the edge preserving ability of these methods

The associate editor coordinating the review of this manuscript and approving it for publication was Shiqi Wang.

is poor. Wavelet thresholding-based methods can be divided into soft threshold and hard threshold [16]. Hard threshold method preserves local features like signal edge, but the signal will be distorted as a whole. Soft threshold processing is relatively smooth, but it may cause local distortion like blurred signal edge. Nonlocal mean (NLM) filtering provides a new idea in image denoising, it utilizes the whole image for denoising. The principle of this method is to find similar regions in the image by using image blocks as units and then averages these regions, which can remove the Gaussian noise well. One of the most successful extensions of nonlocal technique for SAR despeckling is SAR blocking-matching 3-D (SAR-BM3D) [17] which combines nonlocal filtering with wavelet-domain shrinkage. This method achieves the state-of-the-art despeckling performance for SAR images but like other nonlocal algorithms, it cannot preserve the edges well in the homogeneous area. Moreover, the huge computational burden is another disadvantage.

In recent years, a large number of variational models [18]–[20] have been widely designed to multiplicative noise removal and have been proven to be effective for removing speckle noise of SAR images. The variational model for image denoising is based on the idea of variational method [21]. After determining the energy function of the image, the image can be smoothed by minimizing the energy function. Usually, the variational model contains regularization term and data fidelity term. Due to the edge preserving and noise removing properties, total variation (TV) regularizer [2], [22] has been widely used. Besides, the speckle noise is usually described by different density function such as Poisson, Rayleigh and Gamma distribution function [23]. The variational model (RLO model) for speckle noise removal was first presented by Rudin *et al.* [24]. In this model, the structure of image is modeled as a function belonging to the bounded variation(BV) space and often causes the staircase effect. That's to say, the RLO model can not preserve good details. Then in [25], Aubert and Aujol proposed a new variational model (AA model) via the maximum a posteriori estimator for Gamma noise. The defect of this model is that it lacks the global convexity. In order to overcome this problem, Shi and Osher introduced a strictly convex general model (SO model) using the inverse scale space [26]. In brief, the data fidelity terms [19], [27] in the above models are widely used in speckle noise removal and additive noise removal [28]. However, since TV-based models suffer from staircase effect [29] in the flat areas which may lead to the loss of some structures, many methods have been proposed to reduce the blocky effect. One of the improved methods is the high-order Partial Differential Equations(PDEs) method [30]. Different from TV regularization, the basis of high-order variational models is to minimize the derivatives of the image [31], [32]. The high-order regularizations mainly include Laplace Δu regularization [33], bounded Hessian $\nabla^2 u$ regularization [34], total curvature (TC) $\nabla \cdot \left(\nabla u / |\nabla u|\right)$ regularization [35] as well as total generalized variation(TGV) regularization [36], [37]. In a word, with the denoising models mentioned above, it is difficult to remove the image noise and keep the appropriate details simultaneously only with a single model. Thus some researchers proposed some hybrid models to preserve image details while avoiding the staircase effect [38], [39]. In [38], the authors combined fractional-order total variation with high-order Laplace term. The authors in [39] proposed a convex model consisting of the Kullback-Leiber divergence as the data fidelity term, the total variation and high-order total variation (Hessian) as regularization term. However, the statistical property of the noise in these existing variational models is not fully considered. They are only suitable for homogeneous regions because of the assumption that the underlying terrain RCS is equivalent to a constant. The research of radar cross sectional area (RCS) [40] is an important content of SAR image processing. RCS mainly reflects the scattering characteristics of ground objects to radar waves, so the research of RCS is helpful for SAR image interpretation of ground objects. Above all, most of the SAR image scenes include inhomogeneous regions where the RCS fluctuations need to be considered.

With the above considerations, the difficulties of effective speckle noise removal method lie in the reasonable data fidelity design with statistical property of the speckle noise, preserving edges details and avoiding the staircase effect. So the objective of this paper is to construct a variational model combining the first-order TV regularization with high-order TC regularization, and replacing the classical fidelity terms with targeted fidelity term. Moreover, Mellin transform based method is applied to estimate the parameters and we design a fast numerical algorithm for the proposed model.

The rest of this paper is organized as follows. Section II reviews the statistical properties of SAR images and introduces the related variational models briefly. In section III, we derive our new model to denoise images corrupted by speckle noise and give the process of the Mellin transform-based parameters estimation. In section IV, alternating minimization iterative scheme and numerical approximation methods for solving the proposed variational models are detailedly presented. The validation experimental results on synthetic and real SAR images are demonstrated in Section V. Section VI is the conclusion of this paper.

II. RELATED PREVIOUS WORKS

The goal of this section is to briefly introduce the statistical properties of the speckle noise. Noteworthily, the amplitude image normally is converted into intensity image through the square root operation. Comparing with the intensity domain, despeckling in the amplitude domain can achieve better results [41]. So the focus of this paper is on the amplitude image.

A. STATISTICAL PROPERTIES OF THE SPECKLE NOISE

The SAR image degradation process could be mathematically modeled by

$$f = u\eta \tag{1}$$

where $f(x) : \Omega \rightarrow R^{m\times n}$ represents the noise image, $u : \Omega \rightarrow R^{m\times n}$ is the original image and η denotes speckle noise. Ω is the image domain, R is the image space with size of $m \times n$. u and η are independent random variables. Besides, without loss of generality, we assume that entries of u and η are positive in the noise model. The amplitude speckle noise is assumed to follow a Gamma distribution with mean one and its probability density function is given by

$$P_\eta(\eta) = \frac{2L^L}{\Gamma(L)}\eta^{2L-1}e^{-L\eta^2}\ \eta, \quad L > 0 \tag{2}$$

where L is the equivalent number of looks. $\Gamma(\cdot)$ is the Gamma function.

B. RELATED VARIATIONAL MODELS

This section briefly reviews the related variational models for multiplicative noise removal. Based on the assumption that multiplicative noise follows the Gamma distribution, using Bayesian formula with variational method, Aubert et al proposed a variational model(named AA model) for multiplicative noise removal from non-texture images:

$$\min E(u) = \min\left\{\int_\Omega |\nabla u|\,dxdy + \lambda\int_\Omega (\frac{f}{u} + \log(u))dxdy\right\} \tag{3}$$

where the former is the TV regularization term. Because of the nonconvex character, the solution of Eq.(3) is not the global optimal and the accuracy of the solution also depends on the initialization.

Shi and Osher proposed a strictly convex general model(named SO model) using the relaxed inverse scale space flows. Through logarithm transform, the multiplicative noise is transformed to additive noise:

$$\log f = \log u + \log \eta \tag{4}$$

Then the TV regularization term $|\nabla u|$ is replaced by $|\nabla \log u|$. Let $w = \log u$, a general TV model for speckle noise removal can be achieved:

$$\min E(w) = \min\left\{\begin{array}{l}\int_\Omega |\nabla w|\,dxdy + \\ \lambda\int_\Omega (f\cdot e^{-w} + w)dxdy\end{array}\right\} \tag{5}$$

Based on the TV regularization term and different fidelity terms, several models have been presented for the multiplicative noise removal [22], [42]. Although the above models can reduce the noise effectively while preserving image edge, they will produce staircase effect in smooth areas. Besides, the existing variational models almost ignore the statistical property of the noise and assumed that the underlying terrain RCS is equivalent to a constant, thus they are only suitable for homogeneous regions. However, most SAR image scenes include inhomogeneous regions where the RCS fluctuations should be considered.

C. THE G^0 DISTRIBUTION

Several statistical models have been presented to describe the property of SAR images. Among them, the G^0 distribution proposed by Frery *et al.* [43] is suitable for extremely inhomogeneous regions. Then it was verified that G^0 distribution can accurately model SAR images which have different heterogeneities. Besides, comparative studies of statistical models [44] show that the G^0 distribution outperforms almost all other models for all resolutions. Thus in this paper, we apply the G^0 distribution to model the statistical property of SAR images.

The characteristics of G^0 distribution are as follows: the amplitude backscatter follows the reciprocal of the square root of Gamma distribution and the speckle noise obeys the square root of Gamma law [45]. The density of the reciprocal of the square root of Gamma distribution is given by

$$P(u) = \frac{2}{\gamma^\alpha\Gamma(-\alpha)}u^{2\alpha-1}e^{-\frac{\gamma}{u^2}}, \quad -\alpha, \gamma, u > 0 \tag{6}$$

We can obtain the amplitude G^0 distribution through Eq.(1), Eq.(2), and Eq.(6), which is expressed by the following density

$$P(f) = \frac{2L^L\Gamma(L-\alpha)\,\gamma^{-\alpha}f^{2L-1}}{\Gamma(L)\,\Gamma(-\alpha)(\gamma+Lf^2)^{L-\alpha}}, \quad -\alpha, \gamma, L, f > 0 \tag{7}$$

Here, the parameter α represents roughness of the observed area, and γ is a scale parameter which is bound up with the intensity of the backscatter. The G^0 distribution can model SAR images which have different inhomogeneities [46] precisely by setting different parameters.

III. PROPOSED MODEL

In this section, we propose our variational model for speckle noise removal and present the parameters estimation process.

A. THE DATA FIDELITY TERM

Inspired by the literature [45] and combine the contents described above, the new data fitting function is reached as follows:

Firstly, combining Eq.(1) and Eq.(2), the following conditional probability density function is obtained:

$$P(f|u) = \frac{2L^Lf^{2L-1}e^{-L\left(\frac{f}{u}\right)^2}}{\Gamma(L)u^{2L}}, \quad L, f > 0 \tag{8}$$

where u is assumed to have a priori as in Eq.(6) and through Bayesian MAP rule, it is preferred to maximize $P(u|f)$. Applying Eq.(6) and Eq.(8) to the Bayesian formula, the following equation is obtained

$$\begin{aligned} P(u|f) &= \frac{P(f|u)P(u)}{P(f)} \propto \prod P(u)P(f|u) \\ &\propto \prod u^{2\alpha-2L-1}e^{-\frac{\gamma+Lf^2}{u^2}} \end{aligned} \tag{9}$$

where $\propto$ denotes "proportional to". Because all the quantities are positive, it is amount to maximize the log-function. That is to say, minimizing the minus log-function:

$$-\log(P(u|f)) \propto \int\left[(2L-2\alpha+1)\log(u) + \frac{\gamma+Lf^2}{u^2}\right] \tag{10}$$

Thus we can obtain the new data fitting function

$$\int \left[(2L - 2\alpha + 1)\log(u) + \frac{\gamma + Lf^2}{u^2} \right] \tag{11}$$

B. THE REGULARIZER TERM

The TV regularizer is a classical regularizer which is proposed by Rudin Osher and Fatemi. It is usually expressed as $|\nabla u|$, and ∇u means first-order derivative which can be discretized as $\nabla u = \begin{bmatrix} \partial x^+ u \\ \partial y^+ u \end{bmatrix}$. This $|\nabla u|$ is anisotropic, that is to say, the operator does not diffuse along the gradient direction, but only along the orthogonal direction of the gradient. So it can effectively protect image details such as edge and texture while denoising.

Although TV regularizer performs well in denoising process. In the actual process of image processing, there is no edge in the flat area of the image. So when using it to process the image, the diffusion along the edge direction will leads to false edges, which will also appears the so-called ladder effect. To attack this problem, high-order [47] regularization were introduced. Among them, the Laplace Δu regularization, bounded Hessian $\nabla^2 u$ regularization and TC $\nabla \cdot \left(\nabla u / |\nabla u|\right)$ regularization are all second-order and the TC is the most complex. The TC regularization was first introduced by Nitzberg and Mumford [48] in early 1990s. Many related researches [10], [49] on additive noise removal have been done before. Above all, because of the computational complexity, little research has been done on TC regularization for speckle noise removal.

In this paper, the typical TV regularizer and the complex TC regularizer is employed as our regularization term(named hybrid regularization).

C. THE PROPOSED MODEL

In this subsection, considering the new data fitting function Eq.(11), combing it with the above hybrid regularization as well as adding boundary detection function more precisely, the proposed speckle noise removal model aims to minimize the following energy.

$$\begin{aligned} \min E(u) = {} & \theta_1 \int_\Omega g(x) \left| \nabla \cdot \frac{\nabla u}{|\nabla u|} \right| dx + \theta_2 \int_\Omega g(x) |\nabla u| \, dx \\ & + \theta \int_\Omega \left((2L - 2\alpha + 1)\log(u) + \frac{\gamma + Lf^2}{u^2} \right) dx \end{aligned} \tag{12}$$

By the combination of TV and TC regularization, the enhanced model overcomes the staircase effect caused by TV regularization as well as the low efficiency caused by TC regularization, and fully utilizes their advantages respectively. It means that this new model can preserve fine image details such as edge and texture at the same time reducing speckle noise.

In this model, α and γ are the parameters which need to be estimated. When $\alpha = 1$ and $\gamma = 0$, the fidelity term is similar to the fidelity of AA model. θ_1, θ_2 are the penalty parameters imposed on the TC and TV regularizer term respectively to control the smoothness level of the resulting clean image. θ is a positive parameter which balances the action between the regularization term and the data fidelity term. Boundary detection function $g(x)$ is used to prevent blurring the image edge.

Let

$$g(x) = \left\{ \begin{array}{ll} 1, & n = 1 \\ \dfrac{1}{\left|\nabla z^{(n-1)}(x)\right|}, & n \geq 2 \end{array} \right\} \tag{13}$$

n is the number of external iterations, function Eq.(13) is determined by the gradient size of $\left|\nabla z^{(n-1)}\right|$. In the larger edge area of $\left|\nabla z^{(n-1)}\right|$, function Eq.(13) is relatively small and smoothness constraints have less weight, thus it can achieve the goal of preserving edges. On the contrary, in the smaller smooth region of $\left|\nabla z^{(n-1)}\right|$, function Eq.(13) is relatively big and the weight of smoothness constraint is large, thus it can achieve the purpose of noise removal. To prevent the denominator of Eq.(13) from being zero, we rewrite Eq.(13) as

$$g(x) = \left\{ \begin{array}{ll} 1, & n = 1 \\ \dfrac{1}{1 + \left|\nabla z^{(n-1)}(x)\right|}, & n \geq 2 \end{array} \right\} \tag{14}$$

To overcome the lack of global convexity, we set $z = \log u$ for the new model and transform it into the following globally convex model.

$$\begin{aligned} \min E(z) = {} & \theta_1 \int_\Omega g(x) \left| \nabla \cdot \frac{\nabla z}{|\nabla z|} \right| dx + \theta_2 \int_\Omega g(x) |\nabla z| \, dx \\ & + \theta \int_\Omega \left((2L - 2\alpha + 1) z + \left(\gamma + Lf^2 \right) e^{-2z} \right) dx \end{aligned} \tag{15}$$

Although the combination of TC regularization term and TV regularization has high effectiveness in removing staircase effect and preservation of image features, the minimization of the corresponding functional Eq.(15) is a very challenging problem. Here, auxiliary variables $w, q, \vec{p}, \vec{n}, \vec{m}$ are introduced to simplify Eq.(15) as following energy functional:

$$\begin{aligned} \min \; E(w) = {} & \theta_1 \int_\Omega g(x)|q| dx + \theta_2 \int_\Omega g(x)|\vec{p}| dx \\ & + \theta \int_\Omega \left((2L - 2\alpha + 1) w + \left(\gamma + Lf^2 \right) e^{-2w} \right) dx \\ \text{s.t. } & w = z, \; \vec{p} = \nabla z, \; \vec{n} = \frac{\vec{p}}{|\vec{p}|}, \; q = \nabla \cdot \vec{n} \end{aligned} \tag{16}$$

Thus, according to the well-known Holder inequality, $\vec{n} = \vec{p}/|\vec{p}|$ can be transformed into $|\vec{n}| \leq 1$ and $\vec{p} = \vec{n} \cdot |\vec{p}|$ equivalent constraints. Then, we obtain $q = \nabla \cdot \vec{n} = \nabla \cdot \left(\nabla z / |\nabla z|\right)$ and the constraint $\vec{m} = \vec{n}$ is designed. Consequently, we get $|\vec{m}| \leq 1$ and $\vec{m}\vec{p} \leq |\vec{p}|$.

By introducing parameters, L^2 penalization is adopted for constraints $w = z, \vec{p} = \nabla z, q = \nabla \cdot \vec{n}, \vec{m} = \vec{n}$. For $|\vec{p}| - \vec{m} \cdot \vec{p}$ is always bigger than 0, we use L^1 penalization for constraint $|\vec{p}| = \vec{m} \cdot \vec{p}$. Thus, the constrained optimization

problem Eq.(16) can be efficiently solved with the following functional.

$$E(z,w,\vec{p},q,\vec{n},\vec{m}) = \underset{z,w,q,\vec{p},\vec{n},\vec{m}}{\arg\min} \begin{Bmatrix} \theta_1 \int_\Omega g(x)|q|\,dx + \theta_2 \int_\Omega g(x)|\vec{p}|\,dx \\ +\theta \int_\Omega \left((2L-2\alpha+1)w + \left(\gamma + Lf^2\right)e^{-2w}\right)dx \\ +\int_\Omega \lambda_1^k (z-w)\,dx + \frac{\mu_1}{2}\int_\Omega (z-w)^2 dx \\ +\int_\Omega \lambda_2^k \left(|\overrightarrow{p}| - \overrightarrow{p}\cdot\overrightarrow{m}\right)dx + \mu_2 \int_\Omega \left(|\overrightarrow{p}| - \overrightarrow{p}\cdot\overrightarrow{m}\right)dx \\ +\int_\Omega \overrightarrow{\lambda_3^k}\left(\overrightarrow{p} - \nabla z\right)dx + \frac{\mu_3}{2}\int_\Omega \left(\overrightarrow{p} - \nabla z\right)^2 dx \\ +\int_\Omega \lambda_4^k \left(q - \nabla\cdot\overrightarrow{n}\right)dx + \frac{\mu_4}{2}\int_\Omega \left(q - \nabla\cdot\overrightarrow{n}\right)^2 dx \\ +\int_\Omega \overrightarrow{\lambda_5^k}\left(\overrightarrow{n} - \overrightarrow{m}\right)dx + \frac{\mu_5}{2}\int_\Omega |\overrightarrow{n} - \overrightarrow{m}|^2 dx \end{Bmatrix} \tag{17}$$

where $\mu_1, \mu_2, \mu_3, \mu_4, \mu_5$ are positive penalty parameters, $\lambda_1, \lambda_2, \vec{\lambda}_3, \lambda_4, \vec{\lambda}_5$ are lagrange multipliers. u denotes the denoised image we need to find, z is the log of u. Dual variable w is the log of u, $\vec{p}$ is a vector valued function related to gradient of the function u. q is a scalar valued function related to divergence of vector function $\vec{n}$, $\vec{n}$ is a vector valued function related to the unit vectors of the level curves of u, $\vec{m}$ is a vector valued function used to relax variable $\vec{n}$.

D. PARAMETER ESTIMATION

In this section, the unknown parameters α, γ involved in the proposed model are estimated according to the multiplicative model of speckle noise and Mellin convolution, which is regarded as an effective estimation method in [50].

Replacing Fourier transform with Mellin transform in general statistics, the corresponding second kind of statistics can be defined. The first and second characteristic function of the second kind are defined as

$$\Phi(s) = \int_0^\infty x^{s-1} f(x)dx, \quad \psi(s) = \ln \Phi(s) \tag{18}$$

respectively. The r-order logarithmic cumulant k_r is given as

$$k_r = \frac{d^r \psi(s)}{ds^r}|_{r=1} \tag{19}$$

Logarithmic cumulant can be estimated by sample logarithmic cumulant. Used the first two order logarithmic cumulants as example, there are

$$\hat{k}_1 = \frac{1}{M}\sum_{i=1}^{M} 2\ln y_i, \quad \hat{k}_2 = \frac{1}{M-1}\sum_{i=1}^{M}\left(2\ln y_i - \hat{k}_1\right)^2 \tag{20}$$

where y_i is samples, M is the numbers of samples.

By substituting the probability density function of the G^0 distribution into Eq.(18) and Eq.(19) and conduct appropriate simplification, we can obtain the parameters estimation equations

$$\begin{aligned} k_1 &= \ln\left(\gamma/L\right) + \psi(L) - \psi(-\alpha), \\ k_2 &= \psi(1,L) + \psi(1,-\alpha) \end{aligned} \tag{21}$$

where L is the equivalent number of looks, $\psi(\cdot)$ is the digamma function, $\psi(1,\cdot)$ is the first-order polygamma function.

Then the parameters of proposed model can be determined according to Eq.(20), Eq.(21)

$$\begin{aligned} \alpha &= -\psi^{-1}\left(\hat{k}_2 - \psi(1,L)\right), \\ \gamma &= L\exp\left(\hat{k}_1 + \psi(-\alpha) - \psi(L)\right) \end{aligned} \tag{22}$$

where $\psi^{-1}(\cdot)$ is the inverse of the first order polygamma function.

IV. FAST NUMERICAL ALGORITHMS

The numerical approximation algorithms for speckle noise removal mainly contain fixed point method [51], semi-implicit iteration [52], dual method [53], Split Bregman algorithm [54] and so on. In this paper, the alternating direction method of multipliers (ADMM) [55] is used to design a fast numerical approximation iterative scheme.

A. PRELIMINARIES

In order to solve the variational model proposed above, let us introduce the discretization of first-order and second-order operators for convenience. Let $\Omega \to R^{M\times N}$ represent the two-dimensional grey scale image space Ω with size $M \times N$. The coordinates x and y are oriented along rows and columns, respectively. So the first-order forward differences of u at point (i,j) can be written as

$$\begin{aligned} \partial_x^+ u_{ij} &= \begin{cases} u_{i+1,j} - u_{i,j} & if\ 1 \le i < M \\ u_{1,j} - u_{M,j} & if\ i = M, \end{cases} \\ \partial_y^+ u_{ij} &= \begin{cases} u_{i,j+1} - u_{i,j} & if\ 1 \le j < N \\ u_{i,1} - u_{i,N} & if\ j = N \end{cases} \end{aligned} \tag{23}$$

The first-order backward differences are as follows

$$\begin{aligned} \partial_x^- u_{ij} &= \begin{cases} u_{i,j} - u_{i-1,j} & if\ 1 < i \le M \\ u_{1,j} - u_{M,j} & if\ i = 1, \end{cases} \\ \partial_y^- u_{ij} &= \begin{cases} u_{i,j} - u_{i,j-1} & if\ 1 < j \le N \\ u_{i,1} - u_{i,N} & if\ j = 1 \end{cases} \end{aligned} \tag{24}$$

Besides, the gradient, Laplacian, gradient of divergence will be implemented for proposed model, which can be discretized as following formula:

$$\nabla u = \begin{bmatrix} \partial_x{}^+ u \\ \partial_y{}^+ u \end{bmatrix} \tag{25}$$

$$\nabla\cdot\nabla z = \left(\partial_x{}^-\partial_x{}^+ + \partial_y{}^-\partial_y{}^+\right)z \tag{26}$$

$$\nabla(\nabla\cdot\overset{\mathrm{r}}{n}) = \begin{bmatrix} \partial_x{}^-\partial_x{}^+ n_1 + \partial_x{}^-\partial_y{}^+ n_2 \\ \partial_y{}^-\partial_x{}^+ n_1 + \partial_y{}^-\partial_y{}^+ n_2 \end{bmatrix}. \tag{27}$$

Figure 1 gives the behavior of the discrete differential operators mentioned above.

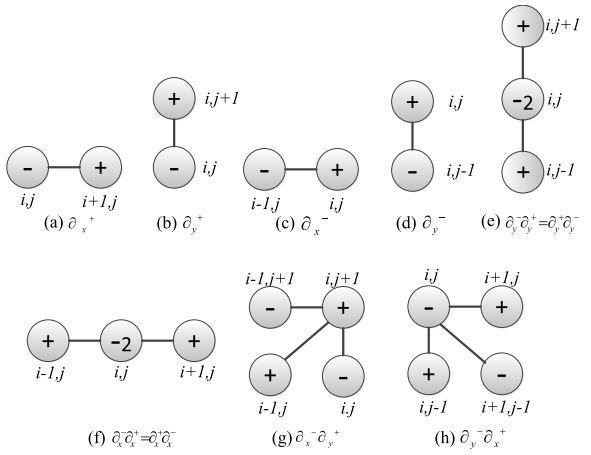

FIGURE 1. Illustration of the discrete first-order and second-order derivative approximations.

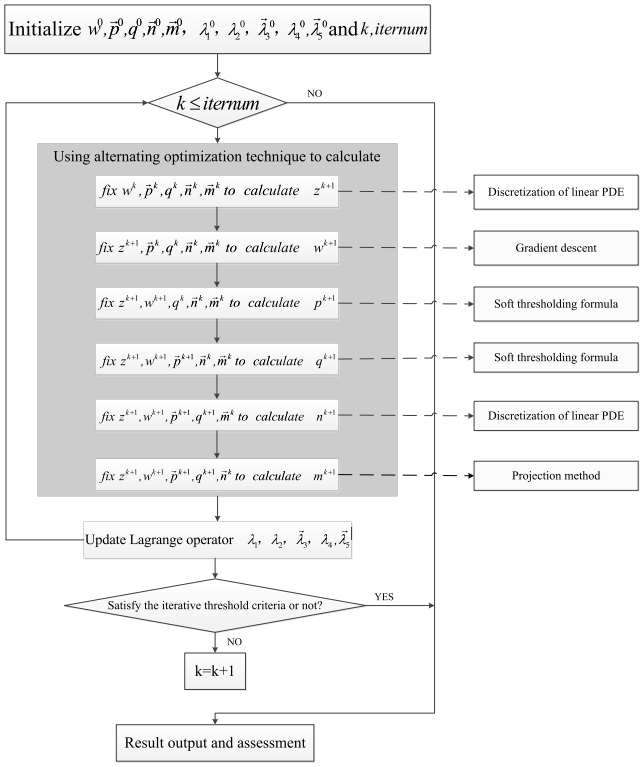

FIGURE 2. Alternating optimization iterative algorithm to solve the problem Eq.(17).

B. FAST NUMERICAL ALGORITHM FOR PROPOSED MODEL

The variables $w^0, \vec{p}^0, q^0, \vec{n}^0, \vec{m}^0$ and Lagrange multipliers $\lambda_1, \lambda_2, \vec{\lambda}_3, \lambda_4, \vec{\lambda}_5$ are simply initialized to zero. When $\log f$ is zero or too small, the computation will be difficult, thus we initialize z^0 as $3\log(f+1)$. The iterative solution process can be read in Figure 2.

1) CALCULATE z

Firstly, in order to calculate z^{k+1}, we need to fix $w^k, \vec{p}^k, q^k, \vec{n}^k, \vec{m}^k$. Then Eq.(17) can be transformed into following function:

$$\varepsilon_1(z) = \int_\Omega \lambda_1^k \left(z - w^k\right) dx + \frac{\mu_1}{2} \int_\Omega \left(z - w^k\right)^2 dx + \int_\Omega \vec{\lambda}_3^k \left(\vec{p}^k - \nabla z\right) dx + \frac{\mu_3}{2} \int_\Omega \left(\vec{p}^k - \nabla z\right)^2 dx \quad (28)$$

The following Euler Lagrange equation can be obtained with respect to z

$$\begin{cases} {\lambda_1}^k + \mu_1\left(z - w^k\right) + \nabla\vec{\lambda}_3^k + \nabla\left(\mu_3\left(\vec{p}^k - \nabla z\right)\right) = 0 & in\Omega \\ \vec{n}\cdot\left[\overrightarrow{\lambda_3^k} + \mu_3\left(\overrightarrow{p}^k - \nabla z\right)\right] = 0 & on\partial\Omega \end{cases} \quad (29)$$

Eq.(29) can be rewritten as

$$\begin{aligned} &\mu_1 z_{ij} - \mu_3\left(z_{i+1j} + z_{i-1j} + z_{ij+1} + z_{ij-1} - 4z_{ij}\right) = g \\ &g = \mu_1 w^k - {\lambda_1}^k - \nabla\vec{\lambda}_3^k - \nabla\mu_3\vec{p}^k \end{aligned} \quad (30)$$

So the final solution can be achieved by the discretization of linear PDE as

$$z_{ij} = \frac{1}{\mu_1 + 4\mu_3}\left[\mu_3\left(z_{i+1j} + z_{i-1j} + z_{ij+1} + z_{ij-1}\right) + g\right] \quad (31)$$

2) CALCULATE w

Secondly, fix $z^{k+1}, \vec{p}^k, q^k, \vec{n}^k, \vec{m}^k$ to calculate w^{k+1}. Eq.(17) can be transformed into:

$$\varepsilon_2(w) = \theta\int_\Omega \left((2L - 2\alpha + 1)w + \left(\gamma + Lf^2\right)e^{-2w}\right) dx + \int_\Omega \lambda_1^k\left(z^{k+1} - w\right) dx + \frac{\mu_1}{2}\int_\Omega \left(z^{k+1} - w\right)^2 dx \quad (32)$$

Then the following Euler equation can be derived:

$$\theta\left((2L - 2\alpha + 1) - 2\left(\gamma + Lf^2\right)e^{-2w}\right) - \lambda_1^k - \mu_1\left(z^{k+1} - w\right) = 0 \quad (33)$$

Here, we especially employ the value of upper step to improve the computation speed. Then w^{k+1} can be simply calculated by gradient descend method as

$$w_{ij}^{k+1} = w_{ij}^k + \begin{bmatrix} \theta\left((2L - 2\alpha + 1) - 2\left(\gamma + Lf^2\right)e^{-2w_{ij}^{k+1}}\right) \\ -\lambda_1^k - \mu_1\left(z^{k+1} - w_{ij}^k\right) \end{bmatrix}\Delta t \quad (34)$$

3) CALCULATE $\vec{p}$

Thirdly, with fixed $z^{k+1}, w^{k+1}, q^k, \vec{n}^k, \vec{m}^k, \vec{p}^{k+1}$ can be calculated by following equation:

$$\begin{aligned} \varepsilon_3\left(\overrightarrow{p}\right) = {} & \theta_2\int_\Omega g(x)\left|\vec{p}\right| dx + \int_\Omega \lambda_2^k\left(\left|\overrightarrow{p}\right| - \overrightarrow{p}\cdot\overrightarrow{m}^k\right) dx \\ & + \mu_2\int_\Omega \left(\left|\overrightarrow{p}\right| - \overrightarrow{p}\cdot\overrightarrow{m}^k\right) dx \\ & + \int_\Omega \overrightarrow{\lambda_3^k}\left(\overrightarrow{p} - \nabla z^{k+1}\right) dx \\ & + \frac{\mu_3}{2}\int_\Omega \left(\overrightarrow{p} - \nabla z^{k+1}\right)^2 dx \end{aligned} \quad (35)$$

Then the Euler equation can be achieved as

$$\left(\theta_2 g(x)+{\lambda_2}^k+\mu_2\right)\frac{\vec{p}}{|\vec{p}|}+\mu_3\left(\vec{p}-\nabla z^{k+1}+\frac{{\vec{\lambda}_3}^k}{\mu_3}-\frac{\left({\lambda_2}^k+\mu_2\right)\vec{m}^k}{\mu_3}\right)=0 \quad (36)$$

Eq.(36) can be easily solved by the analytical soft thresholding equation as

$$\vec{p}^{\,k+1}=\max\left(\left|\vec{S}_{ij}\right|-\frac{A}{\mu_3},0\right)\cdot\frac{\vec{S}_{ij}}{\left|\vec{S}_{ij}\right|},\ 0\frac{\vec{0}}{|\vec{0}|}=0 \quad (37)$$

where $\vec{S}_{ij}=\nabla z^{k+1}-\frac{{\vec{\lambda}_3}^k}{\mu_3}+\frac{\left({\lambda_2}^k+\mu_2\right)\vec{m}^k}{\mu_3}$, $A=\theta_2 g(x)+{\lambda_2}^k+\mu_2$.

4) CALCULATE q

Fourthly, by fixing $z^{k+1}, w^{k+1}, \vec{p}^{k+1}, \vec{n}^k, \vec{m}^k$, we can calculate q^{k+1} with following equation

$$\varepsilon_4(q)=\theta_1\int_\Omega g(x)|q|\,dx+\int_\Omega\lambda_4^k\left(q-\nabla\cdot\vec{n}^k\right)dx+\frac{\mu_4}{2}\int_\Omega\left(q-\nabla\cdot\vec{n}^k\right)^2dx \quad (38)$$

The Euler equation of Eq.(38) is

$$\theta_1 g(x)\frac{q}{|q|}+\mu_4\left(q-\nabla\cdot\vec{n}^k+\frac{\lambda_4^k}{\mu_4}\right)=0 \quad (39)$$

The soft thresholding equations is also employed to solve the problem

$$q^{k+1}=\max\left(\left|\vec{B}_{ij}\right|-\frac{\theta_1 g(x)}{\mu_4},0\right)\frac{\vec{B}_{ij}}{\left|\vec{B}_{ij}\right|},\ 0\frac{\vec{0}}{|\vec{0}|}=0 \quad (40)$$

where $\vec{B}_{ij}=\nabla\vec{n}^k-\frac{{\lambda_4}^k}{\mu_4}$.

5) CALCULATE $\vec{n}$

Fifthly, by fixing $z^{k+1}, w^{k+1}, \vec{p}^{k+1}, q^{k+1}, \vec{m}^k$ to calculate $\vec{n}^{k+1}$, the following equation can be derived

$$\varepsilon_5(\vec{n})=\int_\Omega\lambda_4^k\left(q^{k+1}-\nabla\cdot\vec{n}\right)dx+\frac{\mu_4}{2}\int_\Omega\left(q^{k+1}-\nabla\cdot\vec{n}\right)^2dx+\int_\Omega\vec{\lambda}_5^k\left(\vec{n}-\vec{m}^k\right)dx+\frac{\mu_5}{2}\int_\Omega\left|\vec{n}-\vec{m}^k\right|^2dx \quad (41)$$

The Euler equation of Eq.(41) is

$$\begin{cases}\nabla\left[\mu_4\left(q^{k+1}-\nabla\cdot\vec{n}\right)+{\lambda_4}^k\right]+\vec{\lambda}_5^k+\mu_5\left(\vec{n}-\vec{m}^k\right)=0 & in\Omega\\ \vec{n}\cdot\left[\mu_4\left(q^{k+1}-\nabla\cdot\vec{n}\right)+{\lambda_4}^k\right]=0 & on\partial\Omega\end{cases} \quad (42)$$

Here n is a vector, and $\nabla(\nabla\cdot\vec{n})$ can be calculated according to Eq.(27). So the solution of Eq.(42) is as follows

$$n1_{ij}=\frac{1}{2\mu_4+\mu_5}\begin{bmatrix}\mu_4\begin{pmatrix}n1_{i+1j}+n1_{i-1j}+n2_{ij+1}\\+n2_{i-1j}-n2_{i-1j+1}-n2_{ij}\end{pmatrix}\\-\lambda_{51}-\frac{\partial\lambda_4}{\partial x}-\mu_4\left(\frac{\partial q}{\partial x}\right)+\mu_5 m1\end{bmatrix}$$

$$n2_{ij}=\frac{1}{2\mu_4+\mu_5}\begin{bmatrix}\mu_4\begin{pmatrix}n2_{i+1}j+n2_{i-1j}+n1_{i+1}j\\+n1_{ij-1}-n1_{i+1}j-1-n1_{ij}\end{pmatrix}\\-\lambda_{52}-\frac{\partial\lambda_4}{\partial y}-\mu_4\left(\frac{\partial q}{\partial y}\right)+\mu_5 m2\end{bmatrix} \quad (43)$$

6) CALCULATE $\vec{m}$

Finally, with fixed $z^{k+1}, w^{k+1}, \vec{p}^{k+1}, q^{k+1}, \vec{n}^{k+1}$, we can calculate $\vec{m}^{k+1}$ and obtain the following equation

$$\varepsilon_6(\vec{m})=\int_\Omega\lambda_2^k\left(|\vec{p}|-\vec{p}\cdot\vec{m}\right)dx+\mu_2\int_\Omega\left(|\vec{p}|-\vec{p}\cdot\vec{m}\right)dx+\int_\Omega\vec{\lambda}_5^k\left(\vec{n}-\vec{m}\right)dx+\frac{\mu_5}{2}\int_\Omega|\vec{n}-\vec{m}|^2dx \quad (44)$$

Euler equation of Eq.(44) is

$${\lambda_2}^k\vec{p}^{\,k+1}+\mu_2\vec{p}^{\,k+1}+\vec{\lambda}_5^k+\mu_5\left(\vec{n}^{k+1}-\vec{m}\right)=0 \quad (45)$$

Hence, the following projection formulation can be imposed on $\vec{m}$

$$\vec{m}=\begin{cases}\frac{{\lambda_2}^k\vec{p}^{\,k+1}+\mu_2\vec{p}^{\,k+1}+{\lambda_5}^k}{\mu_5}+\vec{n}^{k+1}\ \left|\vec{m}\right|\le 1\\ \frac{{\lambda_2}^k\vec{p}^{\,k+1}+\mu_2\vec{p}^{\,k+1}+{\lambda_5}^k}{\mu_5}+\vec{n}^{k+1}\Big/\left|\frac{{\lambda_2}^k\vec{p}^{\,k+1}+\mu_2\vec{p}^{\,k+1}+{\lambda_5}^k}{\mu_5}+\vec{n}^{k+1}\right|\ \left|\vec{m}\right|>1\end{cases} \quad (46)$$

With all the support functionals of problem Eq.(17) are computed for convex optimization, the ADMM algorithm can be read as follows

V. NUMERICAL EXPERIMENTS

In this section, the denoising performance of the proposed method is verified quantitatively and qualitatively through experimental study on synthetic images degraded by speckle noise and real SAR images. And our proposed method is overall compared with some classical and state-of-the-art SAR despeckling techniques which include Lee filter [14], AA model [25], SO model [26], SAR-BM3D [17] and a TV based speckle removal model [39]. For concise, the model proposed in [39] is named as TVH model. The parameter of compared methods are set as suggested in the reference papers. In the proposed model, the stopping criteria is defined as $\left|E^k-E^{k-1}\right|/E^k<\varepsilon$, where E^k is the energy value of the current step and E^{k-1} is the energy value of previous step. ε is a small tolerance used to stop iteration. $\varepsilon=10^{-3}$ in all cases. All experiments are performed using Matlab 2015b on a windows 10 platform with an Intel Core i3-2120 CPU at 3.30GHz and 4GB memory.

Algorithm 1 ADMM Algorithm for Proposed Model Eq.(17)

01: function $Model_{Despeckling}\,(f)$
02: Initialization: Set $z = 3\log(f+1)$, $w = z$, $(\vec{p}, q, \vec{n}, \vec{m}; \lambda_1, \lambda_2, \vec{\lambda}_3, \lambda_4, \vec{\lambda}_5) = 0$, $(\beta_1, \beta_2, \beta_3, \beta_4, \beta_5, \Delta t, iteration) > 0$
the value of α, γ need to be estimate.
03: repeat
04: Compute z according to Eq.(31)
05: Compute w according to Eq.(34)
06: Compute $\vec{p}$ according to Eq.(37)
07: Compute q according to Eq.(40)
08: Compute $\vec{n}$ according to Eq.(43)
09: Compute $\vec{m}$ according to Eq.(46)
10: Update Lagrange operator
$\lambda_1^{k+1} = \lambda_1{}^k + \mu_1\left(z^{k+1} - w^{k+1}\right)$
11: Update Lagrange operator
$\lambda_2^{k+1} = \lambda_2{}^k + \mu_2\left(\left|\overrightarrow{p}^{k+1}\right| - \overrightarrow{p}^{k+1}\cdot\overrightarrow{m}^{k+1}\right)$
12: Update Lagrange operator
$\vec{\lambda}_3^{k+1} = \vec{\lambda}_3^k + \mu_3\left(\overrightarrow{p}^{k+1} - \nabla u^{k+1}\right)$
13: Update Lagrange operator
$\lambda_4^{k+1} = \lambda_4{}^k = +\mu_4\left(q^{k+1} - \nabla\cdot\overrightarrow{n}^{k+1}\right)$
14: Update Lagrange operator
$\vec{\lambda}_5^{k+1} = \vec{\lambda}_5^k + \mu_5\left(\overrightarrow{n}^{k+1} - \overrightarrow{m}^{k+1}\right)$
15: until convergence of u
16: return $u = e^{z/3} - 1$
17:end function;

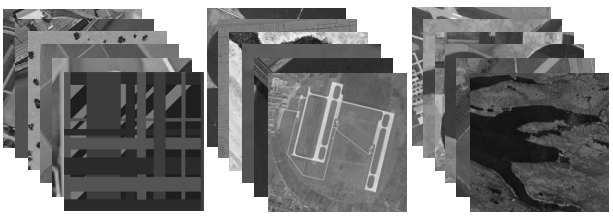

FIGURE 3. Examples of the images.

A. EXPERIMENTAL RESULTS ON SYNTHETIC IMAGES DEGRADED BY SPECKLE NOISE

In this section, the visual and numerical performance of the proposed method are evaluated on the images library which contains 80 images such as Mixedgrid image, Lena image and other 78 images we selected from the NWPU-RESISC45 dataset [56]. Figure 3 shows the examples of the images.

Firstly, Mixedgrid, Farmland, Lena and Chaparral with size 256*256 are selected as test images to evaluate the performance of our proposed method. The original images are shown in Figure 4 (Top). Then the speckle noise code is used to add noise to the original images and we can obtain the corrupted images in Figure 4 (Bottom). The equivalent number of looks on used four original images are 1, 1, 2 and 2 respectively.

The denoising results for images with the Gamma distribution speckle noise are presented in Figure 5. From Figure 5, it can be easily observed that the despeckled images with Lee filter have a lot of residual noise while the other five models show good suppression effect. Due to the application of TV regularization, the results of AA and SO model have staircase effect. Moreover, AA model remains some noise and blurs the images while SO model gives good results since its remaining noise is relatively small. Overall, the despeckling results among the last three models are all desirable. Careful analysis of them reveals that SAR-BM3D and the proposed model can achieve more superior effect than TVH model. Although the SAR-BM3D achieves comparable denoising performance with the proposed algorithm, some ghost artifacts are introduced into the despeckled results which can be clearly seen in the results of the Mixedgrid image and farmland image. By comparison, our proposed model can efficiently enhance visual quality of the images, it not only removes the speckle noise effectively but also preserves the details of the images.

For a local region comparison, in order to see the performance more clearly, we enlarge the regions indicated by red rectangles of Figure 5 into Figure 6. It can be judged that the proposed model provides more natural effect with clearer details. As is seen from the results, Lee filter still has plenty of speckle noise while AA reduces the noise but blurring the images. SO model shows better performance with a little noise remained. Furthermore, AA and SO model generate different degree of staircase effects in the flat region which can be easily observed in the homogeneous region in the Farmland, Lena's hat and the ground of chaparral. The SAR-BM3D suppresses the speckle noise well, but at the same time, it also tends to oversmooth the details of the relative homogeneous region and edges which can be obviously seen in the Mixedgrid image and Farmland image. It is evident that the proposed model reduces the staircase effect and preserves the edges, textures and fine details which can be easily seen in the geometric edge of Mixedgrid image and the dividing line between farmland.

Since the original synthetic images are known, and in order to make the denoising evaluation more objective and convincing, we have made statistics on the common measurements of image fidelity PSNR and SSIM index [57], [58]. PSNR can measure the proximity degree of denoised image to original image and the larger the PSNR value is, the better the result is. SSIM is the indicator to measure the degree of texture, edges and structure preservation. The denoised results can be seen in Table 1 and the best values of PSNR and SSIM are marked in bold. In general, the results are basically the same as those shown above. Table 1 demonstrates that the proposed method can basically obtain the largest PSNR and SSIM values. In summary, the numerical results indicate that the proposed model has the superior performance as SAR-BM3D model with good preservation of edges, texture and fine details.

In order to carry out comprehensive comparison, the experiment is applied on the remaining 76 images in the images library. The test images are corrupted by speckle noise with L equal to 2. Besides, the denoised results are compared with Lee, AA, SO, TVH and SAR-BM3D model. It is worth noting

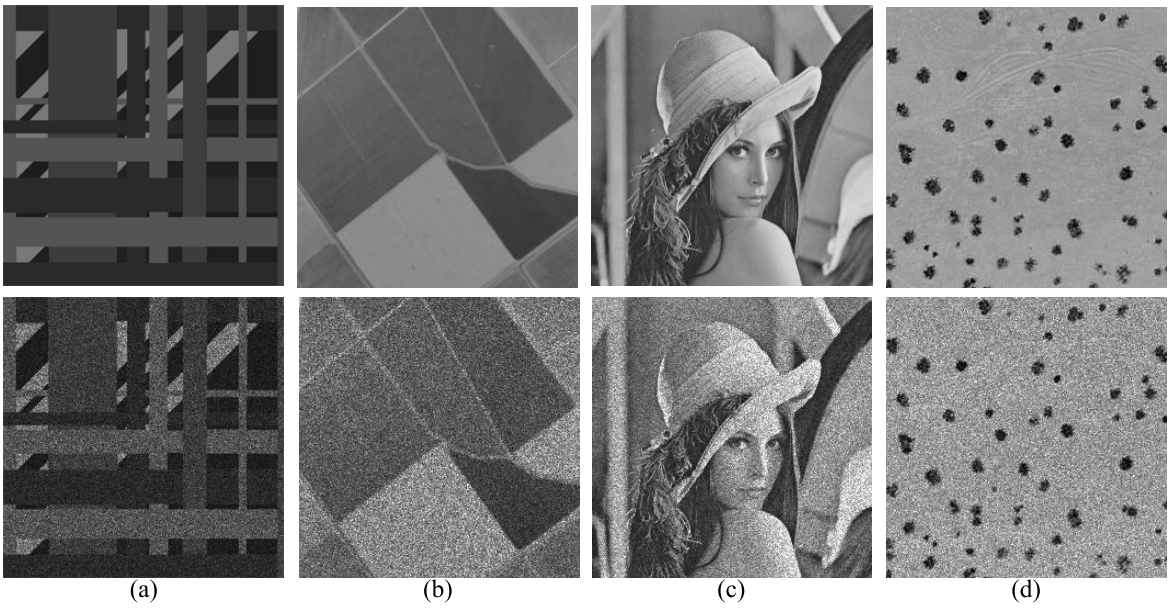

FIGURE 4. Test images. (a) Mixedgrid image. (b) Farmland image. (c) Lena image. (d) Chaparral image.

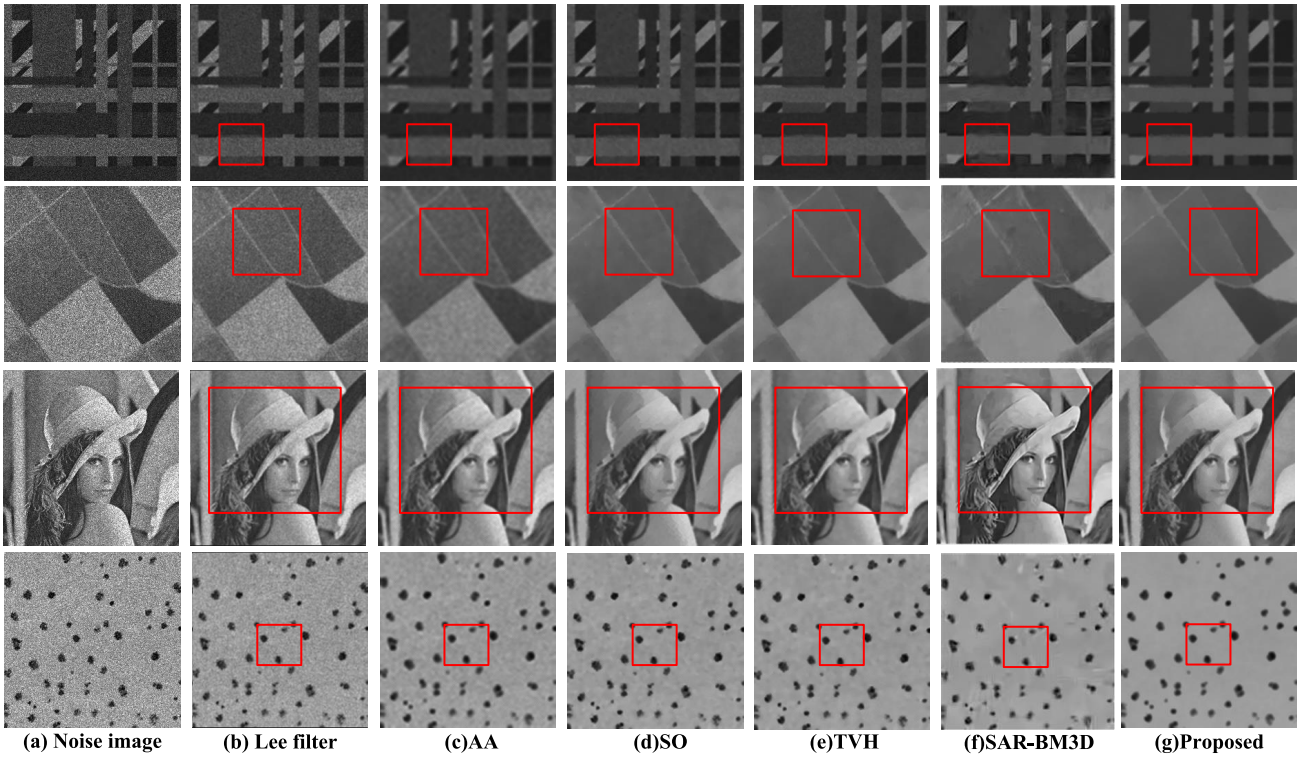

FIGURE 5. The despeckling results of selected four images (a) Gamma noisy image with different Looks(1,1,2,2) (b) Despeckled image by Lee filter (c) Despecked image by AA model (d) Despeckled image by SO model (e) Despeckled image by TVH model (f) Despeckled image by SAR-BM3D model (g) Despeckled image by proposed model.

that all the results are computed per image and then averaged over the image library, see Table 2. The results indicate that our enhanced model has certain advantage compared with previous works.

B. EXPERIMENTAL RESULTS ON REAL SAR IMAGES

In this section, in order to validate the efficiency of the proposed model, we extend the despeckling experiment to real SAR images. The SAR images with different scenes and

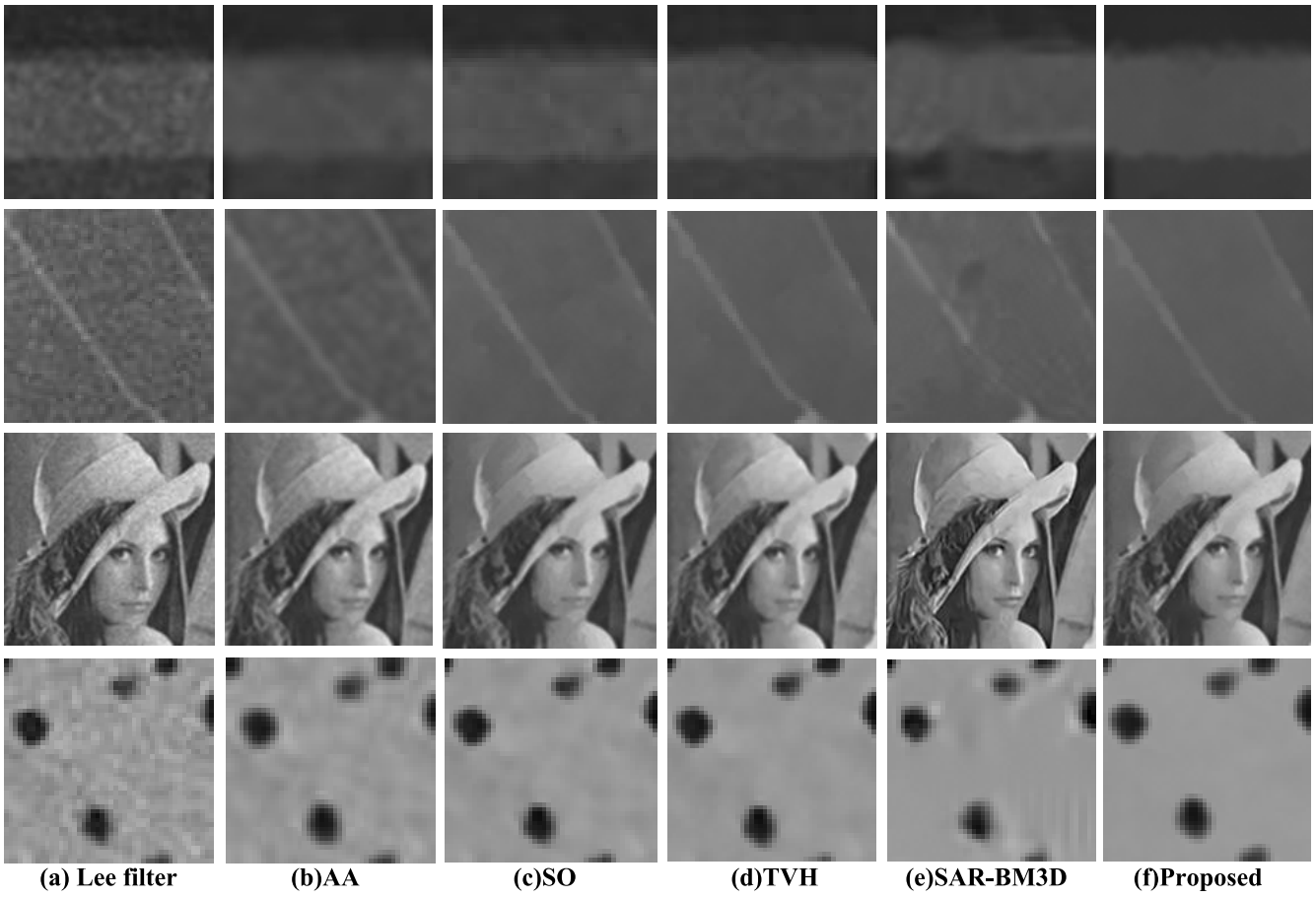

FIGURE 6. Zoom in small sub-regions of images in Figure 5 for detail comparison (a) Lee filter (b) AA model (c) SO model (d) TVH model (e) SAR-BM3D model (f) Proposed model.

TABLE 1. The PSNR and SSIM results of the selected four images.

Method	*Mixed image*		*Farmland image*		*Lena image*		*Chaparral image*	
	PSNR	*SSIM*	*PSNR*	*SSIM*	*PSNR*	*SSIM*	*PSNR*	*SSIM*
Noisy	23.6832	0.4487	20.5234	0.1827	23.5929	0.5421	20.5857	0.2689
Lee	25.8545	0.4868	22.7297	0.2891	24.8583	0.5897	21.9492	0.3302
AA	29.3439	0.8213	30.7997	0.7827	25.9549	0.7211	26.5271	0.6562
SO	30.0975	0.8607	32.2481	0.8760	26.7641	0.7493	27.1784	0.6991
TVH	30.4625	0.8735	33.2475	0.9012	26.9374	0.7501	27.9172	0.7069
SAR-BM3D	**32.5270**	**0.9487**	32.7685	0.8936	**29.3334**	**0.8017**	28.2893	0.7231
Proposed	31.8281	0.9212	**34.1082**	**0.9154**	27.3291	0.7539	**28.4597**	**0.7905**

TABLE 2. The average PSNR and SSIM values of 76 test images.

Method	*Noisy*	*Lee*	*AA*	*SO*	*TVH*	*SAR-BM3D*	*Proposed*
PSNR	22.0963	23.8479	28.1564	29.0720	29.6411	**30.7296**	30.4313
SSIM	0.3608	0.4239	0.7453	0.7963	0.8079	0.8417	**0.8453**

degrees are assumed to follow Gamma noise distribution and they are described briefly as follows:

(1) SAR-1(the first image in the 1st row of Figure 7): a river image regarded as 1 looks, 256*256;

(2) SAR-2(the first image in the 2nd row of Figure 7): a rural area regarded as 1 looks, 256*256;

(3) SAR-3(the first image in the 3rd row of Figure 7): a river-way scene regarded as 2 looks, 256*256;

(4) SAR-4(the first image in the 4th row of Figure 7): a texture region regarded as 3 looks, 256*256.

From the visual appearance of the denoised results in Figure 7, our method are demonstrated better than other models. Analyze the results in detail, we can obtain that Lee filter is not suitable for speckle noise removal with too much noise residues. For AA model, although it has better performance than Lee filter in speckle noise suppression, there are

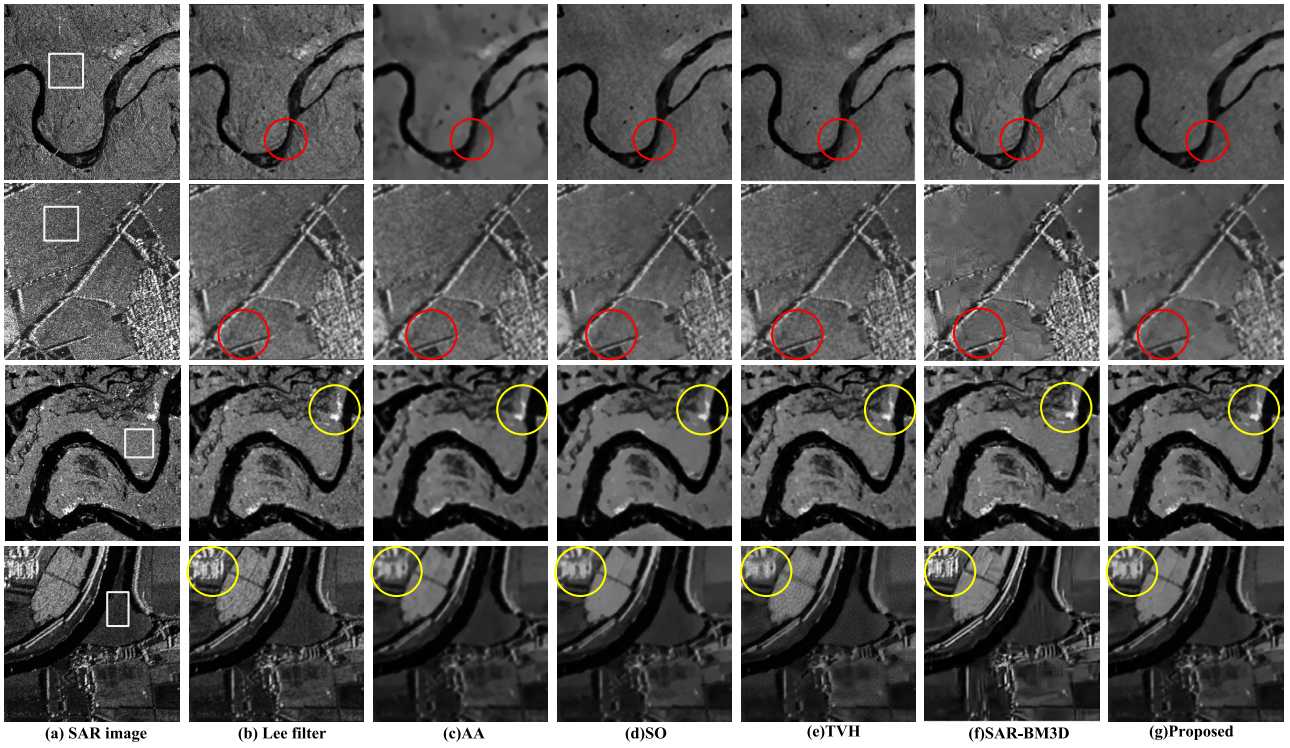

FIGURE 7. The despeckling results of selected four real SAR images (a) SAR image with different Looks(1,1,2,3) (b) Despeckled image by Lee filter (c) Despecked image by AA model (d) Despeckled image by SO model (e) Despeckled image by TVH model (f) Despeckled image by SAR-BM3D model (g) Despeckled image by proposed model.

also some noise remained and the restored images become blurred. By comparison, SO model has pretty good results but has some dark spot in the restored images. Besides, these two TV-based models both cause staircase effect in the flat areas and lose some good details. TVH model repairs the staircase effect in a certain degree but it has some noise residues. The results of SAR-BM3D perform a more conservative despeckling ability compared with the results which were obtained before. In addition, the proposed model strikes a balance between speckle suppression and feature preservation. It can effectively reduce speckle and avoid the staircase effect caused by TV regularization especially in the despeckled performance of the flat region in SAR-1 and SAR-2 (1st row and 2nd row in Figure 7). Besides, benefiting from the character of TC regularization, it can preserve the details well as seen the bright scatters marked by yellow circles and structures like the edges marked by red circles in Figure 7.

Moreover, for the purpose of improving the validity of the results, we present the quantitative evaluation results. ENL(refined equivalent number of looks) [59] was used as our indicator because it can evaluate the degree of speckle removal in a homogeneous region of the recovered image, which is given by $ENL = \mu^2/\sigma^2$, where μ is the mean and σ is the corresponding standard deviation. And larger ENL represents better reduction result. Table 3 presents the values of ENL. We selected uniform regions with size 50*50 for SAR-1,50*50 for SAR-2, 40*40 for SAR-3,50*30 for SAR-4 respectively to compute the ENL. These regions have been pointed by the white rectangles in Figure 7. From Table 3, it is obviously that the largest ENL value is from the proposed model in most cases, which represents that the proposed model occupies a strong speckle reduction ability in homogeneous area. The numerical results seem to be consistent with the visual analysis.

TABLE 3. ENL values of the reduction results for real SAR images.

Images	*SAR-1*	*SAR-2*	*SAR-3*	*SAR-4*
Method	*ENL*	*ENL*	*ENL*	*ENL*
Lee filter	15.7931	11.5741	19.8739	22.6853
AA	44.9650	25.3216	55.4226	64.2599
SO	58.4600	30.3465	63.7453	70.3526
TVH	49.5026	23.8201	52.1081	60.5593
SAR-BM3D	71.3554	**53.7081**	70.8699	85.8151
Proposed	**80.8012**	47.5815	**73.5961**	**92.9287**

C. EDGE PRESERVING RESULTS

Furthermore, horizontal and vertical slices of original, noise and despeckled images about mixedgrid image are presented in Figure 8 and Figure 9 respectively. It can be observed that the despeckled slice curve (red) in (g) almost overlaps with the original slice curve (blue), which demonstrates that the proposed model can preserve the image edge as well as corner. Besides, it can be obtained that the red curves(b-f) generated by other models deviate from original one to varying degrees: the despeckling slice curves(red) from Lee filter

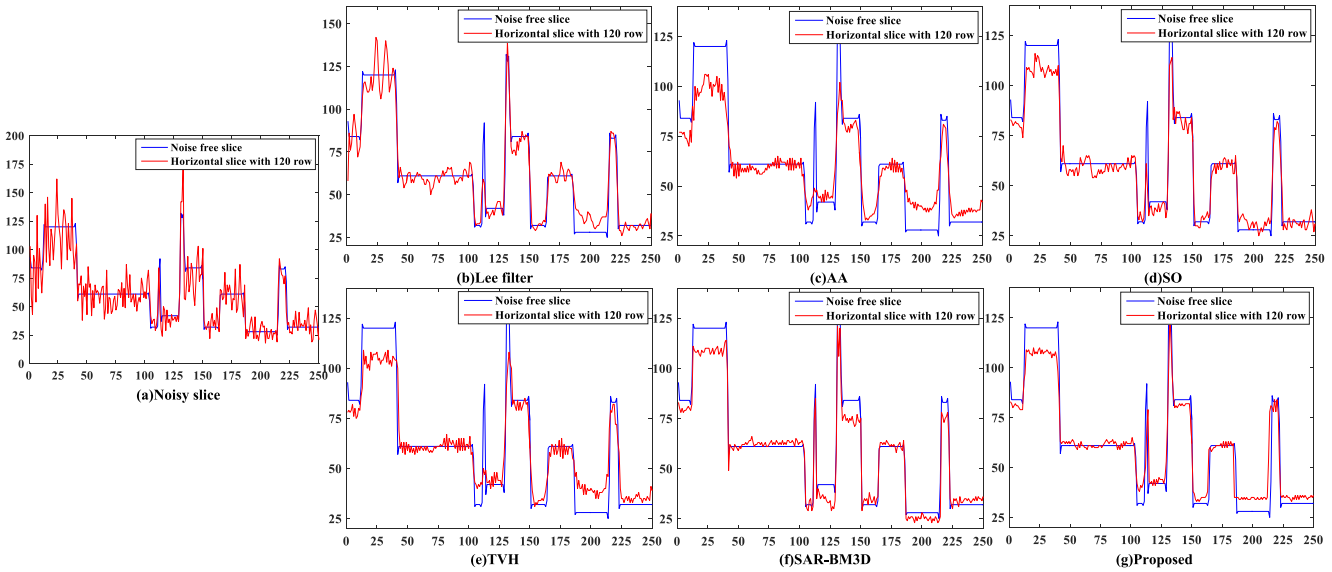

FIGURE 8. Horizontal slices plot of the noisy and denoised mixedgrid image by different models. (a) Noisy slice image; (b) slice of denoised image by Lee filter; (c) slice of denoised image by AA model; (d) slice of denoised image by SO model (e) slice of denoised image by TVH model (f) slice of denoised image by SAR-BM3D model (g) slice of denoised image by Proposed model.

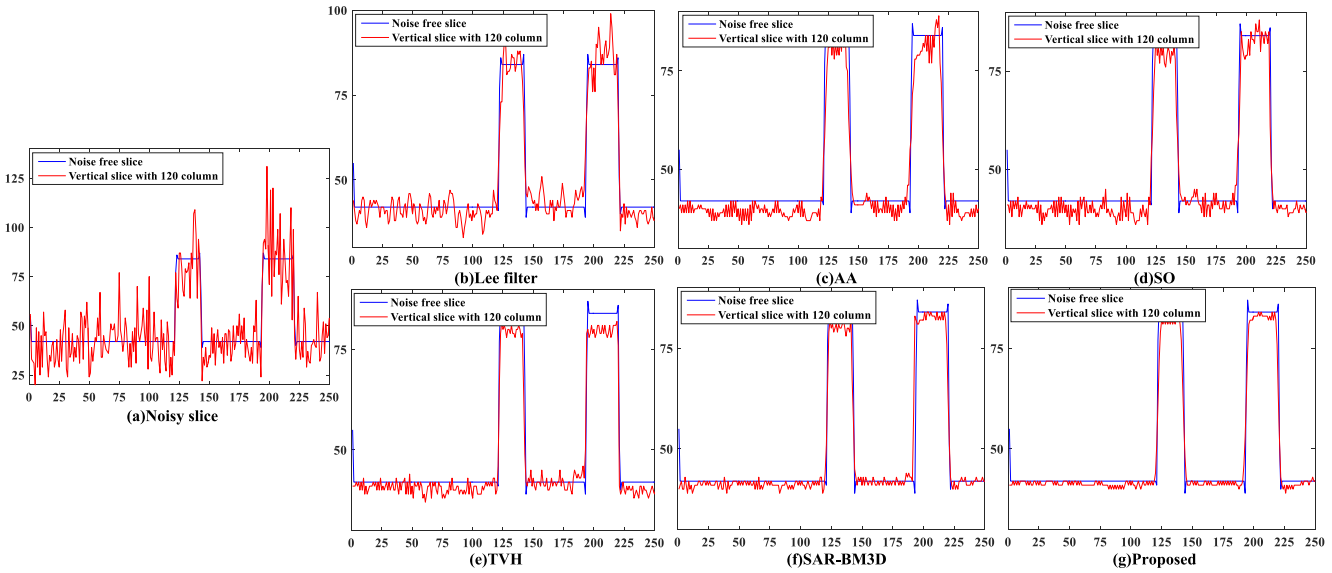

FIGURE 9. Vertical slices plot of the noisy and denoised mixedgrid image by different models. (a) Noisy slice image; (b) slice of denoised image by Lee filter; (c) slice of denoised image by AA model; (d) slice of denoised image by SO model (e) slice of denoised image by TVH model (f) slice of denoised image by SAR-BM3D model (g) slice of denoised image by Proposed model.

fluctuate most while SAR-BM3D performs best in the compared methods. The reason for this phenomenon is the loss of image contrast of different degrees.

D. PARAMETERS' ANALYSIS

The tuning parameters normally have an important influence on despeckling results [38]. The proposed model has three important parameters $\theta, \theta_1, \theta_2$. θ balances the action between the regularization term and the data fidelity term. θ_1 and θ_2 determine the smoothness level of the resulting clean image and we consider the values of θ_1 and θ_2 as equal. Then we can just analyze the effect of the two parameters: θ, θ_1. To conduct the parameter experiment, two images in Figure 4 (Mixedgrid image and Lena image) are corrupted with different levels of speckle(L = 1,2,4) and PSNR is chosen as the index to evaluate the results.

At first, fixing $\theta_1 = 0.08$ and $\theta \in [1, 10]$, the plots of PSNR against different levels of speckle are shown in Figure 10 (top). It is obviously that θ has an important effect on our model's performance. By careful comparison, the regions with higher PSNR values are concentrated in [2,6]. Therefore, in the experiments, the optimal parameter θ is set to 4.

Secondly, fixing the selected θ, and $\theta_1 \in [0.01, 0.55]$, the curves of PSNR are plotted in Figure 10 (bottom).

TABLE 4. Comparison of CPU time of different models on different images.

Method	*Lee filter*	*AA*	*SO*	*TVH*	*SAR-BM3D*	*Proposed*
Images	*Run time(s)*	*Run time(s)*	*Run time(s)*	*Run time(s)*	*Run time(s)*	*Run time(s)*
Mixedgrid	4.5780	4.4723	5.5284	4.3406	1.6602	3.0295
Farmland	4.3904	6.3491	5.7275	3.3595	1.2535	4.9413
Lena	4.5812	5.3961	3.3335	2.6181	4.1006	2.1434
Chaparral	4.5454	3.4036	3.3963	2.6337	1.5352	2.3354
SAR-1	4.5136	3.9174	3.1588	3.0456	1.8697	3.0759
SAR-2	2.9261	1.2972	1.5439	1.4366	1.3720	1.1483
SAR-3	4.5022	1.4326	1.7233	1.5419	1.6796	1.1997
SAR-4	4.4421	1.5150	1.3799	1.1432	1.9732	1.3532
Average	**4.3099**	**3.4729**	**3.2240**	**2.5149**	**1.9305**	**2.4033**

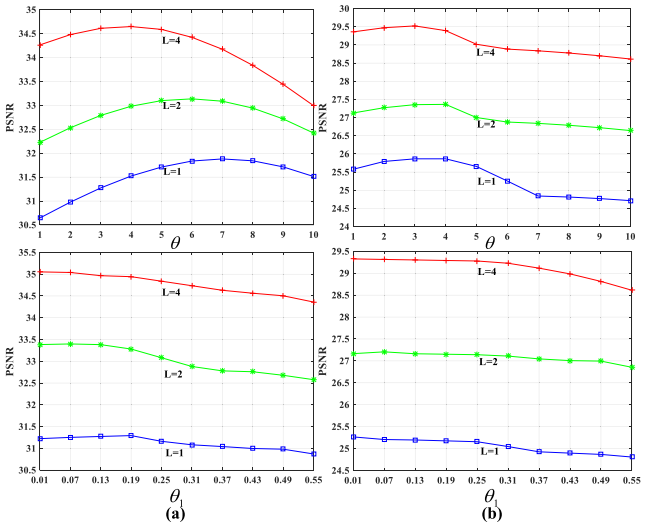

FIGURE 10. (Top) PSNR corresponding to θ when $\theta_1 = 0.08$. (Bottom) PSNR corresponding to θ_1 using selected θ. (a) Mixedgrid image (b) Lena image.

From the plots, we can conclude that the high values of PSNR are mainly distributed in [0.01,0.25]. Moreover, with a careful analyzation, we find the change of PSNR in Lena is smoother while the PSNR values of Mixedgrid image decline obviously after $\theta_1 = 0.19$. Therefore, we set $\theta_1 = 0.13$ as the optimal parameter in the experiments.

E. COMPUTATIONAL EFFICIENCY

For iteration stopping criteria ($\left|E^k - E^{k-1}\right|/E^k < \varepsilon$), threshold $\varepsilon = 10^{-3}$, the runtime which is measured in seconds of experiment images is illustrated in Table 4. The average time is marked in bold. From Table 4, it can be observed that when restoring the synthetic images, SAR-BM3D costs the least time and for real SAR images, our method occupies the best position. Above all, our model has a comparable performance with the state-of-the-art models. That is to say, the run speed of the proposed model is fast which means our algorithm has high efficiency.

VI. CONCLUSION

Despeckling of SAR images is an important issue of image processing which attracts many researchers to develop new methods. In this paper, we aim to propose an enhanced high-order variational model and design its fast algorithm for speckle noise removal. The most relevant contributions are summarized as follows:

(1) The enhanced high-order variational model, based on G^0 distribution, combining TV with TC regularizer and adding boundary detection function, can remove speckle noise while preserving image features.

(2) Because of the proposed model has the characteristics of nonlinearity, non-convexity and high-order derivative. By introducing auxiliary variables, the model is transformed to an alternating optimization convex problem. Meanwhile, the parameters of the model are determined by Mellin transform based on G^0 distribution.

(3) The numerical experiments were conducted through comparative experiments with some classical and state-of-the-art methods. Besides, the results were analyzed subjectively and objectively. Indicators PSNR, SSIM, ENL, slice curves and CPU time were employed to validate the experiment results. Parametric analysis was also included in the experiment.

(4) Finally, the numerical experiments reveal that the proposed variational model can greatly reduce speckle to improve visual quality among the compared method, it not only eliminates staircase effect caused by TV regularization but also preserves the object features such as edge and corner. Besides, numerical results indicate the algorithm can generate good results in terms of computational time.

Noteworthily, SAR image processing occupies an important position in image processing, a lot of works have been carried out with the combination of SAR image denoising. In future work, we will try to integrate speckle noise removal achievements to image segmentation variational model, and will also use much more effective and complicated terms.

ACKNOWLEDGMENT

We would like to thank the anonymous reviewers and the editors for their valuable suggestions and constructive comments which improved the quality of this paper.

REFERENCES

[1] J.-S. Lee, "Speckle suppression and analysis for synthetic aperture radar images," *Opt. Eng.*, vol. 25, no. 5, pp. 636–643, 1985.
[2] M. J. Rycroft, "Book review: Understanding synthetic aperture radar images," *J. Atmos. Solar-Terr. Phys.*, vol. 61, no. 5, p. 424, 1999.
[3] Y. X. Lu, Q. W. Gao, D. Sun, Y. Xia, and D. X. Zhang, "SAR speckle reduction using Laplace mixture model and spatial mutual information in the directionlet domain," *Neurocomputing*, vol. 173, pp. 633–644, Jan. 2016.

[4] M. Tur, K. C. Chin, and J. W. Goodman, "When is speckle noise multiplicative?" *Appl. Opt.*, vol. 21, no. 7, p. 1157, 1982.
[5] R. Sivaranjani, S. M. M. Roomi, and M. Senthilarasi, "Speckle noise removal in SAR images using multi-objective PSO (MOPSO) algorithm." *Appl. Soft Comput.*, vol. 76, pp. 671–681, Mar. 2019.
[6] X. Ma, H. Shen, X. Zhao, and L. Zhang, "SAR image despeckling by the use of variational methods with adaptive nonlocal functionals," *IEEE Trans. Geosci. Remote Sens.*, vol. 54, no. 6, pp. 3421–3435, Jun. 2016.
[7] S.-J. D. Wang and Q.-H. Wang, "Speckle noise suppression method in holographic display using time multiplexing technique," *Opt. Commun.*, vol. 436, pp. 253–257, Apr. 2019.
[8] K. Singh, S. K. Ranade, and C. Singh, "A hybrid algorithm for speckle noise reduction of ultrasound images," *Comput. Methods Programs Biomed.*, vol. 148, pp. 55–69, Sep. 2017.
[9] T. Huang, W. Dong, X. Xie, G. Shi, and X. Bai, "Mixed noise removal via Laplacian scale mixture modeling and nonlocal low-rank approximation," *IEEE Trans. Image Process.*, vol. 26, no. 7, pp. 3171–3186, Jul. 2017.
[10] Y. Mu, B. Huang, Y. Wang, M. Wang, and C. Xue, "Total curvature(TC) model and its alternating direction method of multipliers algorithm for noise removal," *Optoelectron. Lett.*, vol. 15, no. 4, pp. 17–23, 2019.
[11] A. R. Kher and S. Mitra, "Optimum morphological filtering to remove speckle noise from SAR images," *Image Algebra Morphol. Image Process. IV*, vol. 2030, Jun. 1993. doi: 10.1117/12.146651.
[12] D. Gleich and M. Datcu, "Wavelet-based SAR image despeckling and information extraction, using particle filter," *IEEE Trans. Image Process.*, vol. 18, no. 10, pp. 2167–2184, Oct. 2009.
[13] A. Buades, B. Coll, and J.-M. Morel, "A non-local algorithm for image denoising," in *Proc. IEEE Comput. Soc. Conf. Comput. Vis. Pattern Recognit.*, Jul. 2005, pp. 60–65.
[14] J.-S. Lee, "Digital image smoothing and the sigma filter," *Comput. Vis., Graph., Image Process.*, vol. 24, no. 2, pp. 255–269, 1983.
[15] D. T. Kuan, A. A. Sawchuk, T. C. Strand, and P. Chavel, "Adaptive noise smoothing filter for images with signal-dependent noise," *IEEE Trans. Pattern Anal. Mach. Intell.*, vol. PAMI-7, no. 2, pp. 165–177, Mar. 2009.
[16] K. K. Gupta and R. Gupta, "Despeckle and geographical feature extraction in SAR images by wavelet transform," *ISPRS J. Photogram. Remote Sens.*, vol. 62, no. 6, pp. 473–484, 2007.
[17] S. Parrilli, M. Poderico, C. V. Angelino, and L. Verdoliva, "A nonlocal SAR image denoising algorithm based on LLMMSE wavelet shrinkage," *IEEE Trans. Geosci. Remote Sens.*, vol. 50, no. 2, pp. 606–616, Feb. 2012.
[18] P. Liu and X. Liang, "Efficient multiplicative noise removal method using isotropic second order total variation," *Comput. Math. Appl.*, vol. 70, no. 8, pp. 2029–2048, 2015.
[19] S. Li, G. Wang, and X. Zhao, "Multiplicative noise removal via adaptive learned dictionaries and TV regularization," *Digit. Signal Process.*, vol. 50, pp. 218–228, Mar. 2016.
[20] R. W. Liu, L. Shi, W. Huang, J. Xu, S. C. Yu, and D. Wang, "Generalized total variation-based MRI Rician denoising model with spatially adaptive regularization parameters," *Magn. Reson. Imag.*, vol. 32, no. 6, pp. 702–720, Jul. 2014.
[21] B. Shi, L. Huang, and Z. F. Pang, "Fast algorithm for multiplicative noise removal," *J. Vis. Commun. Image Represent.*, vol. 23, no. 1, pp. 126–133, 2012.
[22] Y. Zhao, J. G. Liu, B. Zhang, W. Hong, and Y. R. Wu, "Adaptive total variation regularization based SAR image despeckling and despeckling evaluation index," *IEEE Trans. Geosci. Remote Sens.*, vol. 53, no. 5, pp. 2765–2774, May 2015.
[23] R. Chan, H. Yang, and T. Zeng, "A two-stage image segmentation method for blurry images with poisson or multiplicative gamma noise," *SIAM J. Imag. Sci.*, vol. 7, no. 1, pp. 98–127, 2014.
[24] L. Rudin, P. L. Lions, and S. Osher, "Multiplicative denoising and deblurring: Theory and algorithms," in *Geometric Level Set Methods in Imaging, Vision, and Graphics*. New York, NY, USA: Springer, 2003, pp. 103–119.
[25] G. Aubert and J.-F. Aujol, "A variational approach to removing multiplicative noise," *SIAM J. Appl. Math.*, vol. 68, no. 4, pp. 925–946, 2008.
[26] J. Shi and S. Osher, "A nonlinear inverse scale space method for a convex multiplicative noise model," *SIAM J. Imag. Sci.*, vol. 1, no. 3, pp. 294–321, 2008.
[27] L. Xiao, L. L. Huang, and Z. H. Wei, "A Weberized total variation regularization-based image multiplicative noise removal algorithm," *EURASIP J. Adv. Signal Process.*, vol. 2010, 2010, Art. no. 490384. doi: 10.1155/2010/490384.
[28] N. Chumchob, K. Chen, and C. Britoloeza, "A new variational model for removal of combined additive and multiplicative noise and a fast algorithm for its numerical approximation," *Int. J. Comput. Math.*, vol. 90, no. 1, pp. 140–161, 2013.
[29] F. Li, C. Shen, J. Fan, and C. Shen, "Image restoration combining a total variational filter and a fourth-order filter," *J. Vis. Commun. Image Represent.*, vol. 18, no. 4, pp. 322–330, 2007.
[30] H. M. Reza, "An anisotropic fourth-order diffusion filter for image noise removal," *Int. J. Comput. Vis.*, vol. 92, no. 2, pp. 177–191, 2011.
[31] Y. Hao, J. Xu, S. Li, and X. Zhang, "A variational model based on split Bregman method for multiplicative noise removal," *AEU-Int. J. Electron. Commun.*, vol. 69, no. 9, pp. 1291–1296, 2015.
[32] J. Duan, W. Lu, C. Tench, I. Gottlob, F. Proudlock, N. N. Samani, and L. Bai, "Denoising optical coherence tomography using second order total generalized variation decomposition," *Biomed. Signal Process. Control*, vol. 24, pp. 120–127, Feb. 2016.
[33] Y. Tang, C. Ying, X. Ning, A. Jiang, and Z. Lin, "Image denoising via sparse coding using eigenvectors of graph Laplacian," *Vis. Commun. Image Process.*, vol. 50, pp. 114–122, Mar. 2016.
[34] W. Hinterberger and O. Scherzer, "Variational methods on the space of functions of bounded hessian for convexification and denoising," *Computing*, vol. 76, nos. 1–2, pp. 109–133, 2006.
[35] B. Goldlücke and D. Cremers, "Introducing total curvature for image processing," in *Proc. Int. Conf. Comput. Vis.*, 2011.
[36] J. Duan, Z. Qiu, W. Lu, G. Wang, Z. Pan, and L. Bai, "An edge-weighted second order variational model for image decomposition," *Digit. Signal Process.*, vol. 49, pp. 162–181, Feb. 2016.
[37] J. Duan, W. O. C. Ward, L. Sibbett, Z. Pan, and L. Bai, "Introducing diffusion tensor to high order variational model for image reconstruction," *Digit. Signal Process.*, vol. 69, pp. 323–336, Oct. 2017.
[38] A. Ullah, W. Chen, and M. A. Khan, "A new variational approach for restoring images with multiplicative noise," *Comput. Math. Appl.*, vol. 71, no. 10, pp. 2034–2050, May 2016.
[39] S. Wang, T. Z. Huang, X. L. Zhao, J. J. Mei, and J. Huang, "Speckle noise removal in ultrasound images by first- and second-order total variation," *Numer. Algorithms*, vol. 78, no. 2, pp. 513–533, 2018.
[40] D. U. Sakarya, "Comparison of gimbal approaches to decrease drag force and radar cross sectional area in missile application," *Proc. SPIE, Adv. Opt. Defense Appl., UV through LWIR II*, vol. 10181, May 2017, Art. no. 1018104. doi: 10.1117/12.2264773.
[41] T. Bianchi, F. Argenti, A. Lapini, and L. Alparone, "Amplitude vs intensity despeckling in the wavelet domain using Bayesian estimators," in *Proc. Adv. Radar Remote Sens.*, 2012, pp. 267–274.
[42] F. Yan, F. Fang, H. Liu, and J. Zhu, "Adaptive vectorial total variation models for multi-channel synthetic aperture radar images despeckling with fast algorithms," *IET Image Process.*, vol. 7, no. 9, pp. 795–804, 2013.
[43] A. C. Frery, H.-J. Muller, C. D. C. F. Yanasse, and S. J. S. Sant'Anna, "A model for extremely heterogeneous clutter," *IEEE Trans. Geosci. Remote Sens.*, vol. 35, no. 3, pp. 648–659, May 1997.
[44] M. N. Sumaiya and R. S. S. Kumari, "Comparative study of statistical modeling of wavelet coefficients for SAR image despeckling," *Int. J. Wavelets Multiresolution Inf. Process.*, vol. 15, no. 1, p. 1750003, 2016.
[45] X. Nie, X. Huang, and W. Feng, "A new nonlocal TV-based variational model for SAR image despeckling based on the G^0 distribution," *Digit. Signal Process.*, vol. 68, pp. 44–56, Sep. 2017.
[46] F. Cribari-Neto, A. C. Frery, and M. F. Silva, "Improved estimation of clutter properties in speckled imagery," *Comput. Statist. Data Anal.*, vol. 40, no. 4, pp. 801–824, 2002.
[47] Y. Chen, W. Feng, R. Ranftl, H. Qiao, and T. Pock, "A higher-order MRF based variational model for multiplicative noise reduction," *IEEE Signal Process. Lett.*, vol. 21, no. 11, pp. 1370–1374, Nov. 2014.
[48] M. Nitzberg and D. Mumford, "The 2.1-D sketch," in *Proc. Int. Conf. Comput. Vis.*, 1990, pp. 138–144.
[49] W. Lu, J. Duan, Z. Qiu, Z. Pan, R. W. Liu, and L. Bai, "Implementation of high-order variational models made easy for image processing," *Math. Methods Appl. Sci.*, vol. 39, no. 14, pp. 4208–4233, 2016.
[50] C. Tison, J. M. Nicolas, F. Tupin, and H. Maitre, "A new statistical model for Markovian classification of urban areas in high-resolution SAR images," *IEEE Trans. Geosci. Remote Sens.*, vol. 42, no. 10, pp. 2046–2057, Oct. 2004.
[51] A. Kilicman and M. Wadai, "On the solutions of three-point boundary value problems using variational-fixed point iteration method," *Math. Sci.*, vol. 10, no. 1, pp. 1–8, 2016.
[52] N. F. Loureiro and G. W. Hammett, "An iterative semi-implicit scheme with robust damping," *J. Comput. Phys.*, vol. 227, no. 9, pp. 4518–4542, 2008.

[53] D. Q. Chen, X. P. Du, and Y. Zhou, "Primal–dual algorithm based on Gauss–Seidel scheme with application to multiplicative noise removal," *J. Comput. Appl. Math.*, vol. 292, pp. 609–622, Jan. 2016.
[54] J. Duan, W. Lu, G. Wang, Z. Pan, and B. Li, "Second order variational model for image decomposition using split Bregman algorithm," in *Proc. Int. Conf. Intell. Sci. Big Data Eng.*, 2015, pp. 626–636.
[55] N. Xiong, R. W. Liu, M. Liang, D. Wu, Z. Liu, and H. Wu, "Effective alternating direction optimization methods for sparsity-constrained blind image deblurring," *Sensors*, vol. 17, no. 1, p. 174, 2017.
[56] G. Cheng, J. Han, and X. Lu, "Remote sensing image scene classification: Benchmark and state of the art," *Proc. IEEE*, vol. 105, no. 10, pp. 1865–1883, Oct. 2017.
[57] A. Horé and D. Ziou, "Image quality metrics: PSNR vs. SSIM," in *Proc. Int. Conf. Pattern Recognit.*, 2010, pp. 2366–2369.
[58] B. Huang, Y. Mu, Z. Pan, L. Bai, H. Yang, and J. Duan, "Speckle noise removal convex method using higher-order curvature variation," *IEEE Access*, vol. 7, pp. 79825–79838, 2019.
[59] H. Xie, L. E. Pierce, and F. T. Ulaby, "SAR speckle reduction using wavelet denoising and Markov random field modeling," *IEEE Trans. Geosci. Remote Sens.*, vol. 40, no. 10, pp. 2196–2212, Oct. 2002.

YUNPING MU received the B.S. degree in Internet of Things engineering from Qingdao University, China, in 2017, where she is currently pursuing the M.S. degree. Her research interests include image denoising and segmentation.

BAOXIANG HUANG received the B.S. degree in traffic engineering from the Shandong University of Technology, China, in 2002, the M.S. degree in mechatronic engineering from Shandong University, China, in 2005, and the Ph.D. degree in computer engineering from Ocean University of China, China. She is currently an Associate Professor with the College of Computer Science and Technology, Qingdao University, Qingdao, China, and also an Academic Visitor with the University of Nottingham. Her research interests include remote sensing image processing and analysis, urban acoustic environment modeling, and quality assessment.

ZHENKUAN PAN received the B.E. degree from Northwestern Polytechnical University, Xian, China, in 1987, and the Ph.D. degree from Shanghai Jiao Tong University, Shanghai, China, in 1992. He is currently a Professor with the College of Computer Science and Technology, Qingdao University, Qingdao, China. He has authored or coauthored more than 300 academic papers in the areas of computer vision and dynamics and control. His research interests include variational models of image and geometry processing, and multibody system dynamics.

HUAN YANG received the B.S. degree in computer science from the Heilongjiang Institute of Technology, China, in 2007, the M.S. degree in computer science from Shandong University, China, in 2010, and the Ph.D. degree in computer engineering from Nanyang Technological University, Singapore, in 2015. She is currently a Lecturer with the College of Computer Science and Technology, Qingdao University, Qingdao, China. Her research interests include image/video processing and analysis, perception-based modeling and quality assessment, object detection/recognition, and machine learning.

GUOJIA HOU received the B.S. degree in computer science and the M.S. and Ph.D. degrees in computer applications technology from the Ocean University of China, in 2010, 2012, and 2015, respectively. He is a Lecturer with the College of Computer Science and Technology, Qingdao University. He has authored more than ten journal and conference papers. His current research interests include image processing, image quality evaluation, and pattern recognition.

JINMING DUAN received the Ph.D. in computer science from the University of Nottingham, U.K. From 2017 to 2019, he was a Research Associate with the Imperial College London, U.K. He is currently a Lecturer with the University of Birmingham, U.K. His research interests include deep neural networks, variational methods, partial/ordinary differential equations, numerical optimization, and finite difference/element methods, with applications to image processing, computer vision, and medical imaging analysis.